

OBSERVATIONS OF THE 327 MHz DEUTERIUM HYPERFINE TRANSITION

A. E. E. ROGERS AND K. A. DUDEVOIR

MIT Haystack Observatory, Westford, MA 01886-1299, USA; arogers@haystack.mit.edu

AND

T. M. BANIA

Institute for Astrophysical Research, Boston University, Boston, MA 02215, USA

Received 2006 September 8; accepted 2006 December 14

ABSTRACT

We report measurements of the 327 MHz line of deuterium for regions in the Galactic plane at 171° , 183° , and 195° longitude using an array of 24 stations of fixed phased-antenna elements. The anticenter region was observed using simultaneous multiple beams at each station over a period of just over 2 years from 2004 June to 2006 July. The average deuterium-to-hydrogen (D/H) ratio in the Galactic anticenter region derived from these observations is 21 ± 7 parts per million. The error is $\pm 3 \sigma$ and includes the model-dependency error in conversion of the line amplitudes to the D/H ratio.

Key words: cosmology: observations — Galaxy: general — ISM: abundances — radio lines: ISM — techniques: spectroscopic

Online material: color figures

1. INTRODUCTION

Weinreb (1962) set an upper limit on the deuterium-to-hydrogen (D/H) abundance ratio of 8×10^{-5} by searching for the hyperfine ground-state spin-flip transition of D at 327 MHz (92 cm) in the absorption spectrum of the radio source Cassiopeia A. Weinreb chose Cassiopeia A because the spectrum shows high-opacity absorption features from the similar ground-state spin-flip transition of H at 1420 MHz (21 cm), and the continuum emission using a 26 m diameter dish is strong enough to dominate the system noise. The limit set by Weinreb was determined by the statistical noise that could be achieved in a reasonable amount of observing time. Anantharamaiah & Radhakrishnan (1979) set an upper limit of 5.8×10^{-5} for the line in absorption in the Galactic center and discussed earlier attempts to detect the line toward the Galactic center (Cesarsky et al. 1973; Pasachoff & Cesarsky 1974). Blitz & Heiles (1987) looked for the line in emission toward the Galactic anticenter and set an upper limit of 6×10^{-5} . Heiles et al. (1993) set a limit of 5×10^{-5} from observations of the Galactic center and Cassiopeia A. Chengalur et al. (1997) obtained a marginal detection of the emission from the anticenter to place the D/H ratio between 2.9×10^{-5} and 4.9×10^{-5} . Again, all these observations were limited by the available observing time. In recent years the D/H abundance, which constrains the photon-to-baryon ratio based on the theory of nucleosynthesis during the big bang (Burles et al. 2001), has been measured from the ultraviolet lines in the absorption spectra of stars. However, estimates of the D/H abundance ratio from the ultraviolet Ly α lines have differed by more than a factor of 2. While most of the differences are now thought to be the result of astration and the depletion of D by attachment to interstellar grains (Draine 2004), the small isotopic wavelength shift for the UV D transition could lead to systematic errors due to the line blending with high-velocity H. While all deuterium is thought to have been created by the big bang and only destroyed in stars, Lubowich et al. (1989) searched for the 327 MHz line in regions of stellar activity and set upper limits of D/H of 10^{-3} in these regions.

The array of 24 small radio telescopes shown in Figure 1 was designed and constructed in order to make dedicated, optimally efficient observations of the 327 MHz line. Each telescope, which

is known as a “station,” is a subarray of Yagi elements that form multiple beams simultaneously by appropriate phasing of the individual elements in software. The beamwidth of each station is approximately matched to the latitude extent of the gaseous Galactic plane in order to optimize the D-emission signal from extended regions. Since the stations operate independently and the antennas are spaced far enough apart to make the signals from extended regions uncorrelated, 1 year of observation with the array is equivalent to 24 years of observing with a single station.

We searched for D emission from the direction of the Galactic anticenter and two positions located in the Galactic plane one beamwidth on either side of the anticenter. (We could not observe Cassiopeia A because the stations do not have enough collecting area to obtain a signal that dominates the system noise.) The results of the first year of observation, which resulted in a 6σ detection of the D line and a D/H abundance ratio of $2.3_{-1.3}^{+1.5} \times 10^{-5}$ by number, were reported by Rogers et al. (2005a). Here we present the final results of this experiment, since after 2 years of observing the array has been dismantled. We also give more details of the instrument and the analysis leading to estimates of the D/H abundance ratio in the Galactic anticenter region.

2. INSTRUMENT DESCRIPTION

2.1. 327 MHz Station Subarray

Each station shown in Figure 2 consists of a linear 5×5 (minus one corner element) subarray of 24 active crossed Yagi elements with 0.8 wavelength spacing on a 4.8×4.8 wavelength horizontal ground plane. The Yagis have directors optimized to minimize the gain at the horizon in order to reduce the sensitivity to interference, which mostly comes from the horizon. The beamwidth formed by each station is approximately matched to the extent of the expected deuterium emission.

Low-noise amplifiers (LNAs) are directly connected to the antenna elements, which also form stub filters, as shown in Figure 3. The stub filters are needed to reduce the signal levels from FM radio, TV, and an adjacent digisonde transmitter, which can generate intermodulation products in the LNA. The amplified outputs of the antenna elements are filtered and downconverted to a 50 MHz intermediate frequency and are then digitized and downconverted to



FIG. 1.—View of the 24 stations of the deuterium array. [See the electronic edition of the *Journal* for a color version of this figure.]

baseband. The combination of analog and digital filtering provides more than 100 dB rejection of out-of-band signals. Figure 4 shows the radio spectrum from 70 to 1500 MHz at the location of the array. A block diagram of the station receiver is shown in Figure 5, and the physical layout of the station receiver is shown in Figure 6.

2.2. Receiver Processing

The digital baseband outputs from the antenna elements are converted to spectra using 1024 point complex fast Fourier transforms that are done in the firmware of each digital signal processor (DSP). The data are then transferred via USB cable to motherboard PCs, where they are summed, with appropriate phasing, to provide four simultaneous beams in each polarization. The power spectra from each beam and each antenna element are accumulated and written to disk every 500 s. Corrections for the theoretical response of the digital filters, derived from simulations of the logic of the GC4016 digital downconverter, are made prior to recording the spectra on disk.¹ At the time the array was built it was found necessary to use two motherboard computers, one for

¹ The details of these corrections are given in the technical memoranda associated with the Deuterium Array available at <http://www.haystack.mit.edu>.



FIG. 2.—Close-up of one of the stations with the RFI monitor in the background. [See the electronic edition of the *Journal* for a color version of this figure.]

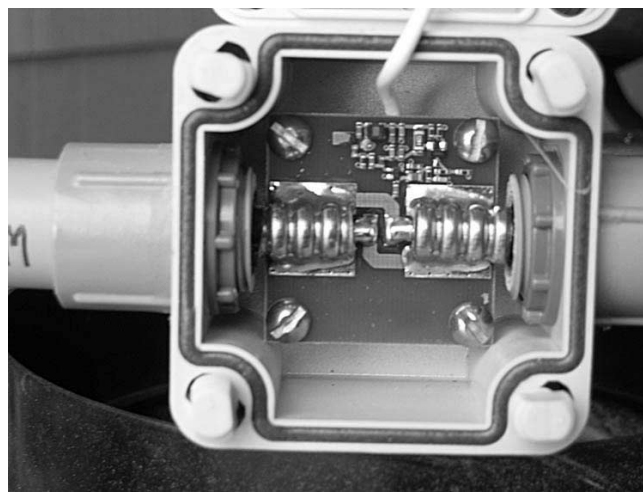


FIG. 3.—Active antenna electronics. Cross-connections to coaxial cable are made so that elements act as antennas and quarter-wave stub filters. [See the electronic edition of the *Journal* for a color version of this figure.]

each polarization. The accumulated spectra from all the stations are then collected each day by a central server.

The station beam-scan performance was measured using the Sun by tilting and orienting the frame to obtain the scan loss in the three principal planes. The results are shown in Figure 7. The receiver noise temperature and collecting area were calibrated by comparing the sidereal variation of a beam pointed at the zenith with a sky model (Rogers et al. 2004). Table 1 summarizes the key characteristics of the array.

2.3. Radio Interference Detection and Reduction

To prevent any signals from the electronics coupling into the antennas, the station receivers are shielded in closed boxes with filtered AC power and fiber optics for communications. A separate radio-frequency interference (RFI) monitoring system consisting of 12 active Yagi antennas pointed every 30° in azimuth, shown in the background of Figure 2, is used to detect sources of interference in the 250 kHz observing band centered at 327.4 MHz (Rogers et al. 2005b). This band is within the 322.0–328.6 MHz radio astronomy band, which is shared with government services. There are no fixed transmitters assigned in this band within 50 km of the array, but there are transient signals, such as occasional unwanted out-of-band emissions from mobile and aeronautical transmitters. These RFI emissions are detected by the monitoring system and then excised from the data. Figure 8 shows a typical set of spectra from the RFI monitor. Most of these transients are spectral in nature. They are detected by setting a threshold of the signal-to-noise ratio (S/N) of 6 in the deviation of a spectral point in 100 s averages. There are, however, occasional broadband

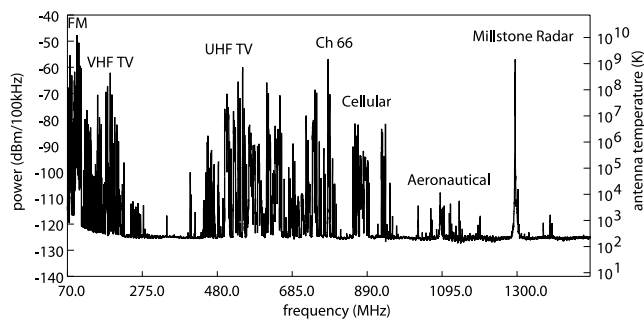


FIG. 4.—Radio spectrum in the environment of the array.

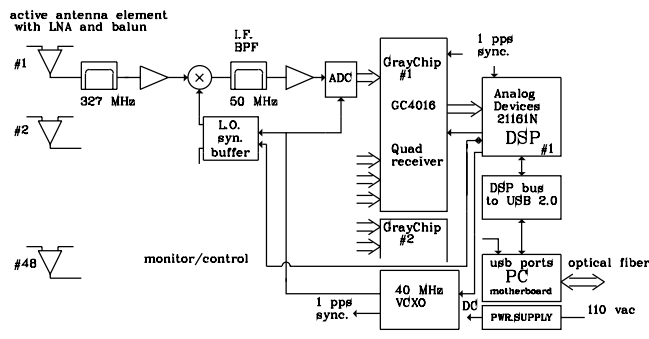


FIG. 5.—Block diagram of the station receivers.

signals that are too weak to be detected by the deviation of any 244 Hz resolution spectral point. These continuum transients are detected by a slope or curvature in the spectra that results from the reception of these signals from multiple paths with different delays. In this case a S/N threshold of 6 in the estimation of the slope and curvature is set for the exclusion of these data.

Continuous-wave (CW) RFI is present from personal computers, digital answering machines, and other electronics in surrounding observatory buildings and adjacent residences. Many of these sources have been located and their emissions reduced by shielding or removal. The effect of the remaining signals is mitigated by the exclusion of their frequencies. Since these signals are much narrower than the expected approximately 20 kHz width of the D line, their exclusion only slightly degrades the S/N of the estimate of the D line's strength. The Yagi antennas of the RFI monitor have a gain of 13 dBi (gain relative to an isotropic antenna), while the horizon response of array Yagis is about -10 dBi. Thus a CW signal with S/N less than 6 from the RFI monitor results in an equivalent signal of less than about 1 part per million (ppm) in the station-beam data. This reduces the effect of RFI that is not detected by the monitor to a level well below that expected from the D line.

Finally, in addition to the RFI monitoring system we use the 500 s integration average spectra from the individual station elements for RFI mitigation. Again, a S/N threshold of 6 is used for transient excision and spectral exclusion.

3. OBSERVATIONS AND DATA REDUCTION

3.1. Observing Schedule

The array runs an automated schedule with three of the four simultaneous beams tracking Galactic longitudes of 171° , 183° ,

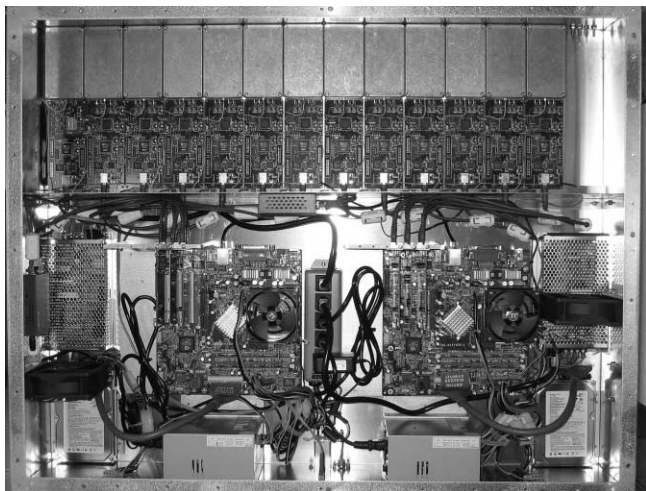


FIG. 6.—Interior of the station receiver. [See the electronic edition of the Journal for a color version of this figure.]

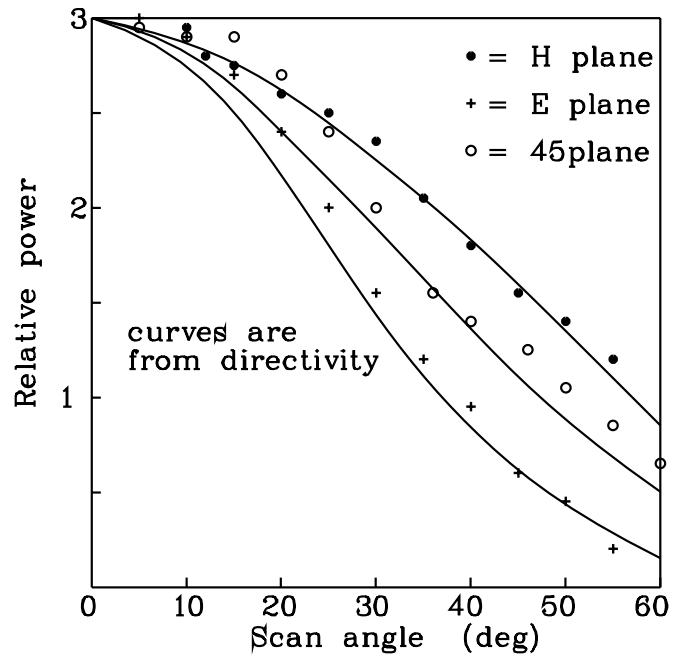


FIG. 7.—Beam-forming scan loss measured in three planes of the station array.

and 195° , and the fourth beam pointed at the zenith. When the anticenter regions are below 50° elevation, other regions at the same declinations but shifted by 6^h , 12^h , and 18^h in right ascension are observed for reference. The Sun, the peak of the continuum in the region of Cygnus, and the pulsar 0329+54 are also observed for short periods each day to provide checks on the phasing of the antenna elements. The primary method of calibration is from the comparison of the zenith-pointed beam with a sky model (Rogers et al. 2004). Except for days when there is snow on the ground planes, the station performance varies very little from day to day. Five hours of observation of the longitudes 171° and 183° and about 3 hr at 195° are obtained each day. Only observations with scan angles (which is the same as the zenith angle for the horizontal orientation of the station ground planes) less than 40° are scheduled, since the aperture efficiency drops below 50% beyond this angle.

3.2. Derivation of the Expected D-Line Strength and Profile

The expected D-line profile was derived from the H I opacity, continuum emission, antenna beam, and system noise. Figure 9 illustrates our method. Shown are maps of the station beam (Fig. 9a), the continuum emission (Fig. 9b) from Haslam et al. (1982) extrapolated to 327 MHz assuming a spectral index of 2.7, and the H I opacity (Fig. 9c) derived from the H I brightness from Hartmann & Burton (1997). The ratio of opacities (τ_D/τ_H) is equal to $0.27(D/H)$, where the factor 0.27 is derived from the ratio of the Einstein A-coefficients and the statistical weights, with some small corrections (Gould 1994) to the values given by Field (1958). We assume that H and D have the same spin temperature (Field 1958) and the same velocity width, since turbulence is the dominant source of the Doppler broadening.

A model for the expected line velocity profile p , which accounts for beam dilution, is derived by the convolution of the antenna beam B with the expected line brightness $s(v, l, b)$, where s is a function of velocity v , Galactic longitude l , and Galactic latitude b . To obtain the expected line spectra as a fraction of total power we normalize with the continuum brightness $T_{\text{cont}}(l, b)$

TABLE 1
SUMMARY OF ARRAY CHARACTERISTICS

Characteristic	Value
Location	Haystack Observatory, Westford, Massachusetts; latitude N42.6°, longitude W71.5°
Array configurations	Quasi-regular array of 24 stations
Station separation.....	Approximately 15 m
Station antenna.....	Compact array of 24 crossed Yagis
Station collecting area	12 m ²
Station beamwidth	14°
Electronic beam steering.....	±40°
Frequency center.....	327.4 MHz
Frequency span.....	250 kHz
Number of spectral channels.....	1024
Resolution	244 Hz
Polarization	Dual linear
System temperature.....	40 K plus sky noise

plus the receiver noise temperature T_R (assuming 40 K from the calibration) so that the profile is given by

$$p = |(s \otimes B) / \{[T_{\text{cont}}(l, b) + T_R] \otimes B\}|. \quad (1)$$

The line brightness from the radiative transfer is a mixture of emission from the spontaneous decay of D atoms and absorption of the background. For small optical depth

$$s(v, l, b) = 0.27(D/H) [T_{\text{spin}} - fT_{\text{cont}}(l, b)] \tau_H(v, l, b), \quad (2)$$

where f is the fraction of continuum behind the interstellar gas, $\tau_H(v, l, b)$ is the hydrogen opacity, and T_{spin} is the spin temperature. The H opacity is derived from the hydrogen-line brightness T_H from the digital data of Hartmann & Burton (1997). The H-line brightness is converted to opacity assuming a constant spin temperature using

$$\tau_H(v, l, b) = -\log_e [1 - T_H(v, l, b)/T_{\text{spin}}]. \quad (3)$$

The beam B is given by the station directivity

$$B = \left| \sum_i e^{i\theta_i(l, b)} \right|^2 d(l, b), \quad (4)$$

where $d(l, b)$ is the power response of each element and $\theta_i(l, b)$ is the phase of the i th element relative to the beam center. The effects of mutual coupling on the beam were considered by Rogers et al. (2004) and found to be negligible.

Table 2 gives the expected peak of the line profile for a range of assumed spin temperatures and locations of the continuum emission. Here we assume a fiducial D/H ratio of 1.5×10^{-5} . The most reasonable assumption, of a 130 K spin temperature and uniform radial mixing of the Galactic continuum (French & Osborne 1976), results in a peak line profile for the array observations toward $l = 171^\circ$, 183° , and 195° of 1.9, 2.6, and 2.0 ppm, respectively. The line velocities toward these regions are -8 , 2 , and 10 , respectively, and the half-power widths are 28, 18, and 20 km s⁻¹, respectively. The estimated profiles shown in Figure 9 and the results given in Table 2 are averages over the range of hour angle of the scheduled observations in order to account for the change in station efficiency with scan angle.

Almost all determinations of the Galactic (D/H) abundance refer to specific objects that have distinct distances from the Sun

and positions in the Galaxy. Our abundances, however, refer to three Galactic anticenter directions that lie in the Galactic plane. In order to estimate the path length of interstellar gas that contributes to the observed D-line emission we used the three-dimensional distribution of gas recently derived by Nakanishi (2005) from H I and CO survey data cubes and assumed Galactic rotation curves. The anticenter line of sight extends out from the Sun through the Local and Perseus arms of the Galaxy. The Nakanishi (2005) H I distribution along this path is very similar to the continuum distribution in models A and B of French & Osborne (1976). This result supports our assumption of uniform mixing in Table 2 as being the most reasonable hypothesis to choose. We estimate, from the data of Figure 5 of Nakanishi (2005), that the column-density-weighted mean distance in the anticenter direction is ~ 3 kpc. The H I column density is about 3×10^{21} H atoms cm⁻² distributed over a distance of ~ 5 kpc. These estimates do not vary significantly from Galactic longitudes of 171° – 195° .

3.3. Maximum Likelihood Estimation of the Line Amplitude

The spectra from each polarization of each station are averaged each day, and a small bandpass-curvature correction is made to all the spectra. This small correction, which is common to all the spectra, accounts for residual effects of the analog electronics and was derived from all the data. Transient signals with S/N greater than 6 in any RFI monitor or array antenna are excised from this average.

The amplitude of the D line is then estimated from a least-squares fit of all the day's data for a given source region. The expected D-line profile is fitted to these data to derive the estimate of the D-line amplitude and a spectral baseline slope and offset. The line-amplitude fit stems from all stations, whereas the slopes and offsets are determined for each station independently. For simplicity the expected D-line profiles are approximated by a Gaussian line shape with the velocity and width from the models derived in § 3.2.

All the daily D-line amplitude estimates were then analyzed. To obtain the maximum likelihood estimate of the D-line amplitude we performed a weighted least-squares solution for the amplitude of the expected line profile as a global parameter. We list in Table 3 the results of the maximum likelihood estimates for the D-line amplitude for observations made over a period of 25 months (2004 June 29 through 2006 July 15). We include reference regions out of the Galactic plane for which no D line is expected.

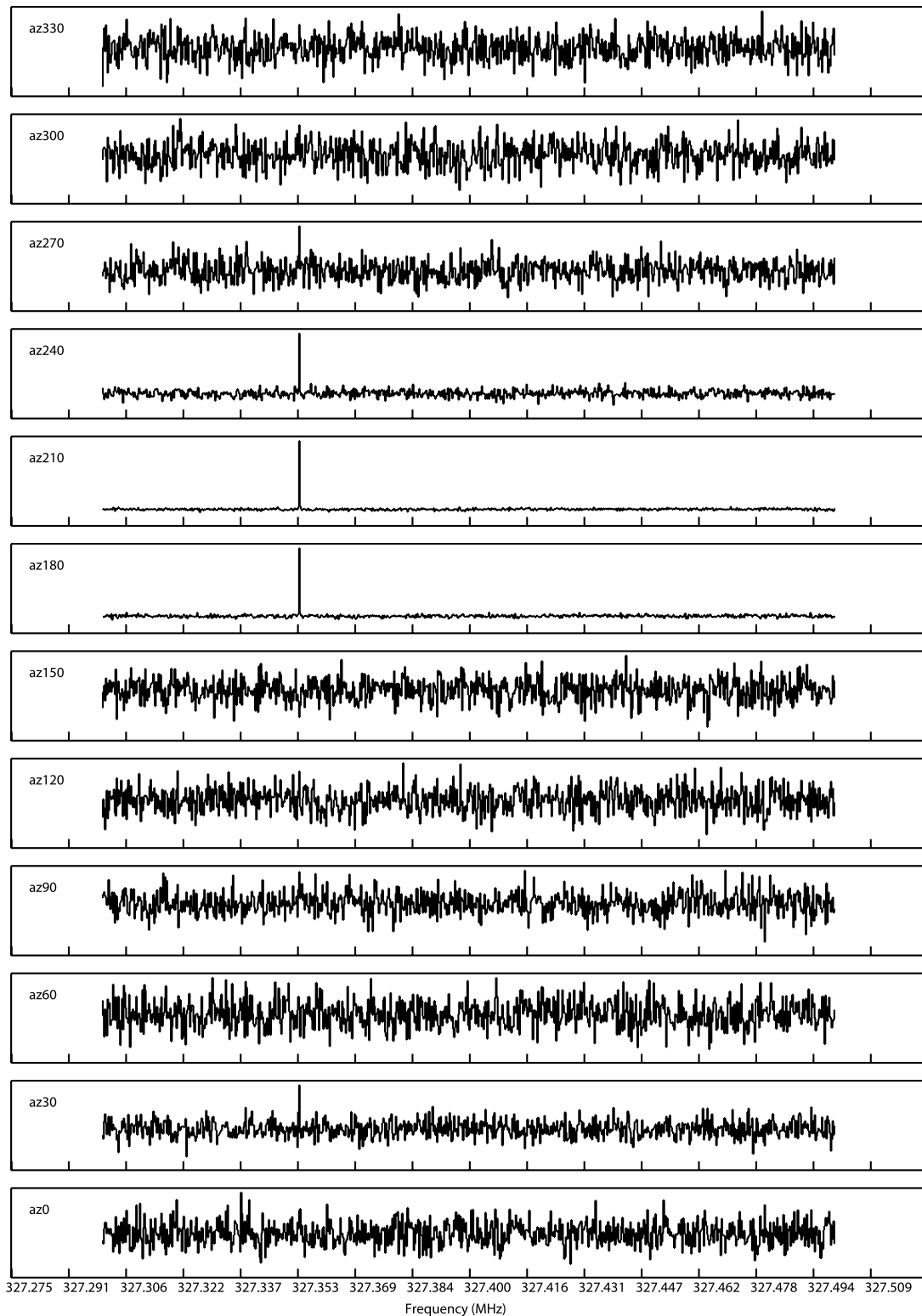


FIG. 8.—Typical spectrum from the 12 Yagi elements of the RFI monitor. The azimuth of the interference is a useful aid in locating the source of interference.

In matrix notation the weighted least-squares solution is given by

$$\hat{x} = (A^T W A)^{-1} A^T W y, \tag{5}$$

where x is a column vector with a single global parameter, representing the D-line amplitude, along with individual local parameters that include a constant offset and slope, for each individual

spectrum from each polarization of each station each day. In addition, y is a column vector of all the spectral data, and W is a diagonal weight matrix whose elements are set to zero for those RFI-afflicted frequency channels that need to be excluded from a given spectrum. The matrix A is the “design” or “steering” matrix.

Since there are approximately 35,000 spectra for each region observed for the 2 years of data the matrix A is extremely large. We

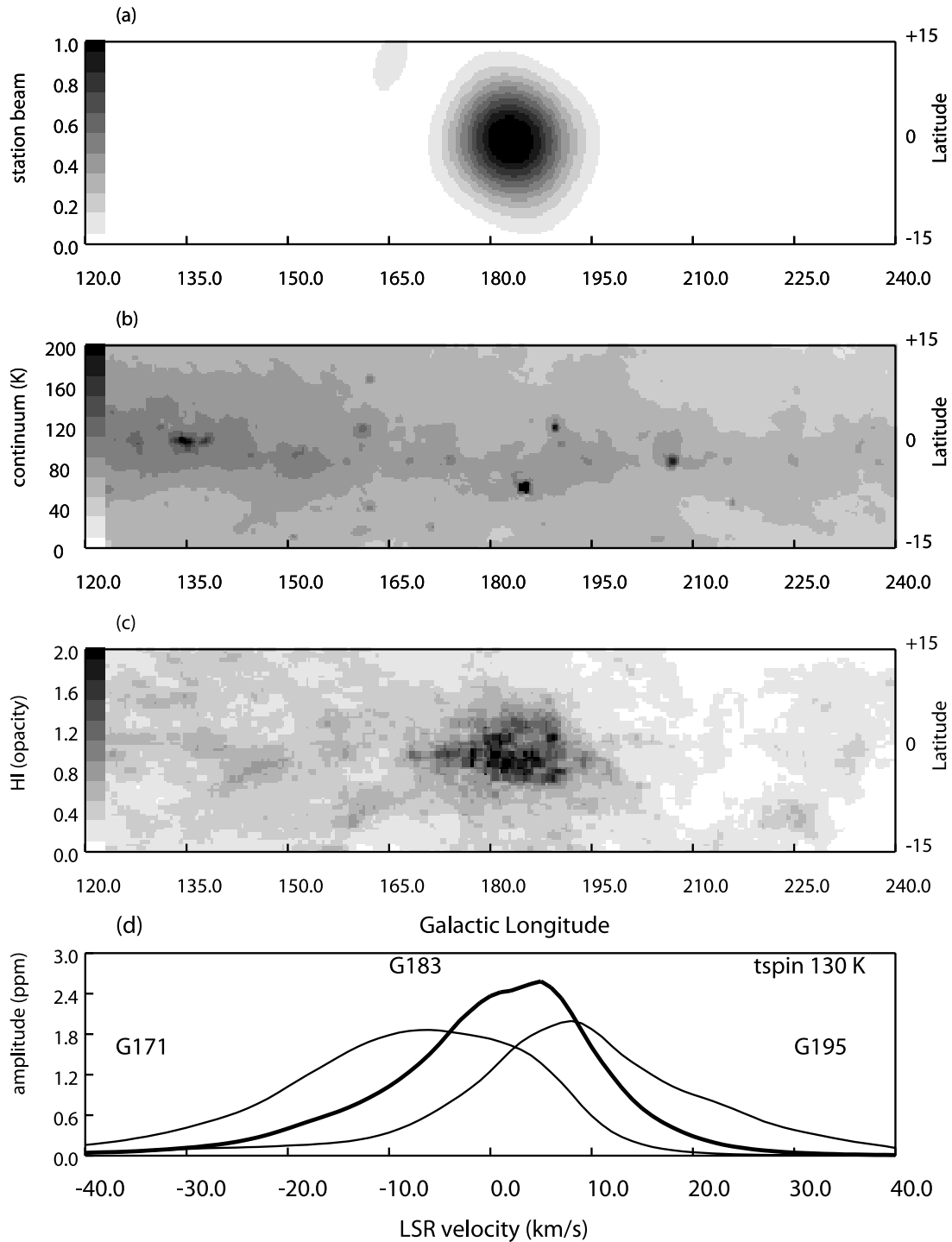


FIG. 9.—Estimated deuterium line profiles. (a) Station beam pattern toward $(l, b) = (183^\circ, 0^\circ)$. (b) Continuum emission in the anticenter region from Haslam et al. (1982). (c) H I opacity (for LSR velocity 0 km s^{-1}) in the anticenter region based on an assumed spin temperature of 130 K from Hartmann & Burton (1997). (d) Estimated D-line profiles (from eq. [1] of § 3.2), in fractional units, for beams toward $l = 171^\circ, 183^\circ,$ and 195° , from the convolution of the line intensities within the station beam. The line intensity is normalized by the total power and hence is plotted in fractional units. The entire data cubes of the continuum and H I data for the full range of Galactic latitude and longitude of the surveys were used in the calculation of these estimated line profiles.

chose to estimate a line amplitude separately for each daily average spectrum and then to perform a weighted average of these amplitudes to obtain the global solution. In this case the weighted least-squares solution for each daily spectrum, designated by index K , is

$$\hat{x}_K = (A_K^T W_K A_K)^{-1} A_K^T W_K y_K, \quad (6)$$

where A_K is the design matrix for an individual spectrum, which is smaller than A . If we designate the first column of A_K as the line

profile, the second as a constant, and the third as a slope, the elements are

$$(A_K)_{i0} = p_{ki}, \quad (7)$$

$$(A_K)_{i1} = 1, \quad (8)$$

$$(A_K)_{i2} = i, \quad (9)$$

where i is the velocity channel index.

TABLE 2
EXPECTED D I PEAK LINE AMPLITUDE

T_{spin} (K)	$(l, b) = (171^\circ, 0^\circ)$			$(l, b) = (183^\circ, 0^\circ)$			$(l, b) = (195^\circ, 0^\circ)$		
	Amp. ^a	Amp. ^b	Amp. ^c	Amp. ^a	Amp. ^b	Amp. ^c	Amp. ^a	Amp. ^b	Amp. ^c
110.....	1.1	2.0	3.0	1.6	2.9	4.3	1.1	2.2	3.3
120.....	1.2	2.0	2.8	1.7	2.8	3.9	1.3	2.2	3.1
130.....	1.2	1.9	2.5	1.7	2.6	3.5	1.3	2.0	2.7
140.....	1.2	1.8	2.4	1.6	2.4	3.2	1.3	1.9	2.5
150.....	1.3	1.8	2.3	1.6	2.3	3.0	1.3	1.8	2.4

NOTE.—Amplitude is the ratio of the signal to system noise in ppm and assumes D/H = 15 ppm by number.

^a Continuum all behind H I.

^b Continuum uniformly mixed with H I with 3 K cosmic microwave background and 3 K extragalactic background.

^c Continuum all in front of H I.

The line profile p_{ki} is calculated each day from the local standard of rest (LSR) and a rest frequency of 327.384352 MHz (Wineland & Ramsey 1972). The D-line amplitude g_k for each spectrum is the first element of \hat{x}_k ,

$$\hat{g}_k = (\hat{x}_k)_0, \tag{10}$$

and

$$\sigma_K = \left[(C_K)_{00} (B T_K)^{-1} \right]^{1/2}, \tag{11}$$

where C_K is the covariance matrix

$$C_K = (A_K^T W_K A_K)^{-1}, \tag{12}$$

B is the resolution of 244 Hz, and T_K is the equivalent single-station integration time in seconds.

The maximum likelihood estimate of the D-line strength is then given by the weighted average global amplitude,

$$\hat{g} = \sum_K (1/\sigma_K^2) \hat{g}_K, \tag{13}$$

TABLE 3
MAXIMUM LIKELIHOOD ESTIMATES OF DEUTERIUM LINE STRENGTH

l (deg)	b (deg)	Amplitude (ppm)	S/N	Integration (yr)
171	0	3.1	8.3	17.5
183	0	3.4	7.4	15.1
195	0	2.4	3.7	7.3
181	69	0.2	0.4	17.4
61	33	0.4	1.1	16.1
104	-23	0.6	1.6	15.4
213	77	-0.1	0.2	15.9
52	24	0.2	0.6	14.9
107	-35	1.4	3.0	16.1
268	77	0.9	1.7	11.2
44	14	1.2	2.0	8.9
112	-46	0.9	0.9	3.7

NOTE.—The integration time is the equivalent single-station integration time (see § 3.2), which is the time a single station with one polarization would take to acquire the same amount of data acquired by the dual-polarized 24 station array (during the period from 2004 June 29 through 2006 July 15) after accounting for the loss of data due to RFI excision.

and variance is given by

$$\sigma = \left[\sum_K (1/\sigma_K^2) \right]^{-1/2}. \tag{14}$$

This method, which separates parameters into local and global parts, is mathematically equivalent to the simultaneous estimation of all the parameters and is in common use in the least-squares analysis of large data sets.

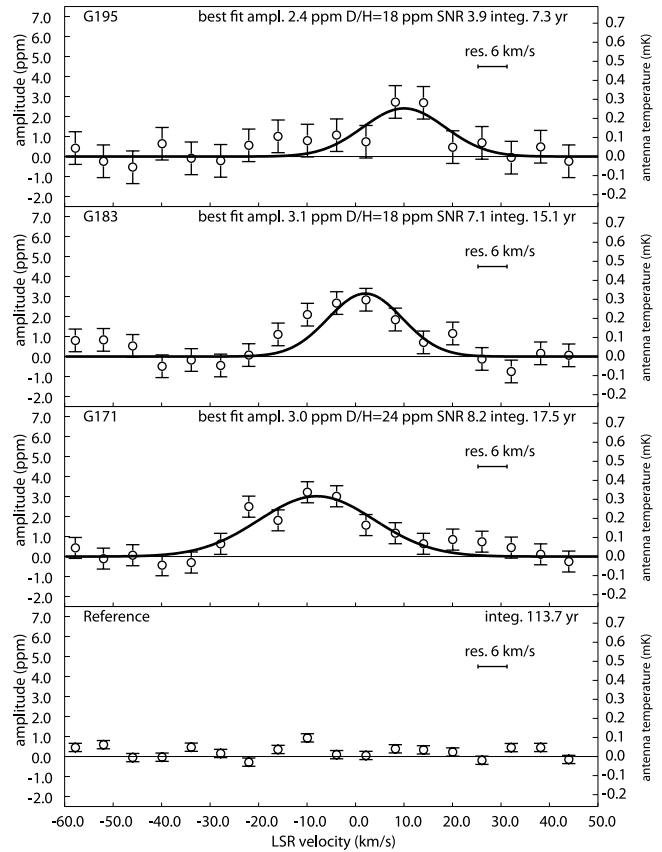


FIG. 10.—Average D spectra for the regions at $(l, b) = (195^\circ, 0^\circ)$, $(183^\circ, 0^\circ)$, $(171^\circ, 0^\circ)$, and the reference regions (top to bottom). The 1σ bars shown on the plots are for the smoothed spectra with resolution of 6 km s^{-1} . The profiles are the best fit with assumed velocities of 10, 2, and -8 km s^{-1} and half-power widths of 20, 18, and 28 km s^{-1} , respectively, as described in § 3.2. An amplitude scale that is the ratio of the signal to system noise is shown in ppm on the left. An antenna temperature scale that is based on an average system noise of 106 K is shown in mK on the right. The integration time given here and in Table 3 is the equivalent single-station integration.

We made an alternate analysis in order to derive the spectra shown in Figure 10. We first smoothed the spectrum from each station for each day and each polarization with a weighted least-squares fit to the original spectrum with the excluded frequencies unweighted. We then derived a small baseline slope and curvature correction using the reference regions and subtracted this correction along with a constant from all the data. The final spectrum for a given source region was obtained from the weighted average of the individual smoothed spectra corrected each day to the LSR for each region. We find that the two methods of analysis give the same D-line amplitude to within about 5%. The second method yields slightly different results due to the effect of the smoothing over regions of unweighted frequencies. Only the first method gives the true maximum likelihood estimate.

All three regions, $l = 171^\circ$, 183° , and 195° , show significant detections of the 327 MHz D transition. Figure 10 shows this average D spectrum along with the least-squares fit to the expected line profile for each of these three regions. Since we know the expected line velocity and width (see § 3.3), a S/N of 7 results in a formal probability of false detection given approximately by $(2\pi)^{-1/2}(S/N)^{-1}e^{-(S/N)^2/2}$, or about 10^{-12} . Figure 10 also shows the average spectrum of the reference regions that lie far from the Galactic plane. Since these reference regions should not show any significant D line, this high $|b|$ spectrum along with the results given in Table 3 provides an indication that the level of systematics in the data is under about 0.4 ppm in line amplitude or 0.04 mK in antenna temperature. The best-fit line profile to the spectrum from the reference regions in Figure 10 corresponds to an upper limit to the systematic error in the (D/H) ratio for the anticenter of 2 ppm. The rms fluctuations in the spectrum of the reference regions are only 0.03 mK.

4. D/H ABUNDANCE IN THE REGION OF THE GALACTIC CENTER

The D/H ratios from the regions at $l = 171^\circ$, 183° , and 195° are 24 ± 3 , 19 ± 2 , and 18 ± 5 ppm, respectively, taken from the D-line amplitudes given in Table 3. The average D/H ratio from all three regions ($l = 171^\circ$, 183° , and 195°) weighted by the inverse noise squared is 21 ± 2 ppm (1 σ errors). If we increase the errors from 1 to 3 σ our estimate is 21 ± 5 ppm. If we include an uncertainty in the spin temperature from 110 to 150 K then our estimate of D/H is 21 ± 7 ppm. We have not formally accounted for the error due to uncertainty in the spatial distribution of the Galactic continuum emission. Here we assume uniform mixing. Although the extreme cases of all the continuum behind or in front of the deuterium are ruled out, there could be some added

contribution to the error from this assumption. Further work is needed to reduce the uncertainty in the spin temperature and distribution of the continuum.

5. DISCUSSION

Ultraviolet absorption measurements of stars within 100 pc of the Sun by the *Far Ultraviolet Spectroscopic Explorer (FUSE)* and *Hubble Space Telescope (HST)* yield D/H ratios close to 15 ppm, but the D/H ratios derived for more distant objects show a large variation. Many *FUSE* abundances for more distant objects are about a factor of 2 lower at ~ 8 ppm (Wood et al. 2004). Quasar lines of sight (Kirkman et al. 2003; Sembach et al. 2004) and some Galactic disk directions, however, have D/H ratios of about 25 ppm, which is consistent with the D/H ratio derived from the baryon density implied by the *Wilkinson Microwave Anisotropy Probe (WMAP)* data (Spergel et al. 2003). The lower D/H abundance in the vicinity of the Sun (Wood et al. 2004) was thought to be due to the destruction of D by astration, but the large variations of the D/H ratio in local regions are now thought to be the result of preferential absorption of D onto grains (Draine 2004, 2006; Linsky et al. 2005, 2006). Thus, undisturbed regions of the interstellar gas may be depleted of D, whereas regions that have been shocked may have a D/H ratio closer to the primordial value divided by the astration factor. Our value of 21 ppm is slightly lower than the cosmological prediction of 25 ppm from *WMAP* data, which could be an indication of some deuterium astration (Romano et al. 2006). Our conservative upper limit of 28 ppm is consistent with the ultraviolet absorption measurements. Our estimate that the D is distributed over ~ 5 kpc in the anticenter direction makes the path length as long as any of the measured optical paths. Thus, our lower limit D/H ratio of 14 ppm, which is significantly higher than the 8 ppm from the *FUSE/HST* measurements for the most distant sources, raises the possibility that there could be systematic errors in either the optical or radio measurements.

We thank Bruce Whittier, Joe Carter, Brian Fanous, Eric Kratzenberg, Richard Jackson, and the technical staff of the observatory for their contributions in the construction of the array. We also thank Preethi Pratap of the observatory staff and Marcos Diaz of Boston University for their work in the development of the RFI monitor. In addition, we thank the reviewer for a careful study of the manuscript, which resulted in the clarification of several key points. Support for the array came from a National Science Foundation grant (ST-0115856), MIT, and TruePosition, Inc.

REFERENCES

- Anantharamaiah, K., & Radhakrishnan, V. 1979, *A&A*, 79, L9
 Blitz, L., & Heiles, C. 1987, *ApJ*, 313, L95
 Burles, S., Nollett, K. M., & Turner, M. S. 2001, *ApJ*, 552, L1
 Cesarsky, D. A., Moffet, A. T., & Pasachoff, J. M. 1973, *ApJ*, 180, L1
 Chengalur, J. N., Braun, R., & Burton, W. B. 1997, *A&A*, 318, L35
 Draine, B. T. 2004, *BAAS*, 36, 614
 ———. 2006, in *ASP Conf. Ser. 348, Astrophysics in the Far Ultraviolet: Five Years of Discovery with FUSE*, ed. G. Sonneborn, H. Moos, & B-G Andersson (San Francisco: ASP), 58
 Field, G. B. 1958, *Proc. IRE*, 46, 240
 French, D. K., & Osborne, J. L. 1976, *MNRAS*, 177, 569
 Gould, R. J. 1994, *ApJ*, 423, 522
 Hartmann, D., & Burton, W. B. 1997, *Atlas of Galactic Neutral Hydrogen* (Cambridge: Cambridge Univ. Press)
 Haslam, C. G. T., Salter, C. J., Stoffel, H., & Wilson, W. E. 1982, *A&AS*, 47, 1
 Heiles, C., McCullough, P. R., & Glassgold, A. E. 1993, *ApJS*, 89, 271
 Kirkman, D., Tytler, D., Suzuki, N., O'Meara, J. M., & Lubin, D. 2003, *ApJS*, 149, 1
 Linsky, J. L., et al. 2005, *BAAS*, 37, 1444
 ———. 2006, *ApJ*, 647, 1106
 Lubowich, D. A., Anantharamaiah, K. R., & Pasachoff, J. M. 1989, *ApJ*, 345, 770
 Nakanishi, H. 2005, *Astron. Herald*, 98, 670
 Pasachoff, J. M., & Cesarsky, D. A. 1974, *ApJ*, 193, 65
 Rogers, A. E. E., Dudevoir, K. A., Carter, J. C., Fanous, B. J., & Kratzenberg, E. 2005a, *ApJ*, 630, L41
 Rogers, A. E. E., Pratap, P., Carter, J. C., & Diaz, M. 2005b, *Radio Sci.*, 40, RS5S17
 Rogers, A. E. E., Pratap, P., Kratzenberg, E., & Diaz, M. 2004, *Radio Sci.*, 39, RS2023
 Romano, D., Tosi, M., Chiappini, C., & Matteucci, F. 2006, *MNRAS*, 369, 295
 Sembach, K. R., et al. 2004, *ApJS*, 150, 387
 Spergel, D. N., et al. 2003, *ApJS*, 148, 175
 Weinreb, S. 1962, *Nature*, 195, 367
 Wineland, D. J., & Ramsey, N. F. 1972, *Phys. Rev. A*, 5, 821
 Wood, B. E., Linsky, J. L., Hebrard, G., Williger, G. M., Moos, H. W., & Blair, W. P. 2004, *ApJ*, 609, 838